EFFECT OF AUSTENITIZATION AND COOLING MEDIUM ON THE MICROSTRUCTURE AND MECHANICAL PROPERTIES OF 12 % MANGANESE STEEL

Salim Khima[1], Rassim Younes[1], Tomków Jacek[2], Abdelhamid Sadeddine[1], Mohand Amokrane Bradai[1], Abderrahim Benabbas[3]

[1]*University of Bejaia, Faculty of Technology*
Laboratory of Mechanics, Materials, and Energetics (L2ME)
06000 Bejaia, Algeria, salim.khima@univ-bejaia.dz (S.K.);
rassim.younes@univ-bejaia.dz (R.Y.);
abdelhamid.sadeddine@univ-bejaia.dz (A.S.);
mdamokrane.bradai@univ-bejaia.dz (M.A.B.).
[2]*Faculty of Mechanical Engineering and Ship Technology Politechnika Gdańska*
Gdańsk University of Technology G. Narutowicza 11/12
80-233 Gdańsk, Poland, jacek.tomkow@pg.edu.pl (J.T.).
[3] *Laboratory Processes for Materials, Energy, Water and Environment*
Faculty of Sciences and Applied Sciences
University of Bouira, 10000 Bouira, Algeria, a.benabbas@univ-bouira.dz (A.B.).

Received 01 May 2025
Accepted 11 November 2025 *DOI: 10.59957/jctm.v61.i2.2026.16*

ABSTRACT

This study evaluates the mechanical properties of high manganese steel used in manufacturing hammers and grinding jaws, which reduce rocks into small particles. Four austenitization heat treatments (1025°C, 1050°C, 1075°C, and 1100°C) were applied, followed by quenching in water and ice water. Samples were characterized for microstructural and structural properties, as well as phase identification, using scanning electron microscopy (SEM) with energy-dispersive spectroscopy (EDS) and X-ray diffraction (XRD). Microhardness measurements revealed an increase in hardness from 436 $HV_{0.2}$ for samples quenched in water at 1025°C to 680 $HV_{0.2}$ for samples quenched in ice water at 1050°C. Impact resistance testing showed a resilience increase from 20 J cm^{-2} for samples treated at 1075°C in water to 161.27 J cm^{-2} for those treated at 1050°C in ice water. Tribological testing indicated a wear rate reduction from 6.23.10^{-4} mg m^{-1} for samples quenched in water to 0.3.10^{-4} mg m^{-1} for samples quenched in ice water. XRD results revealed an austenite solid solution phase across all samples, with additional martensitic and Mn_7C_3 - type carbide phases in those quenched in ice water. SEM analysis confirmed that manganese steel, austenitized for 45 min and quenched in water, shows coarse-grain carbide aggregates within an austenitic matrix. In contrast, samples quenched in ice water exhibit a compact matrix with fine-grain Mn_7C_3 - type carbides and martensite, resulting in enhanced mechanical performance. The 12 % Mn steel, austenitized at 1050°C and quenched in ice water, demonstrated the optimal combination of impact resistance and wear resistance.

Keywords: manganese steel, heat treatment, quenching medium, microstructure, wear and tear.

INTRODUCTION

The he quarries and aggregate industry relies on grinding elements such as hammers and crushing jaws, which are subjected to high mechanical stresses in extreme abrasive conditions. These components, designed to fragment rocks into smaller particles, require both high impact resistance and wear resistance to extend their service life and ensure operational efficiency [1 - 3]. To meet these mechanical and technological demands, these components are frequently manufactured from high-manganese steel, also known as Hadfield steel.

This type of steel contains around 12 % manganese (Mn) as the primary alloying element, providing exceptional toughness and high resistance to shock and abrasion [4 - 7].

The presence of manganese in this steel significantly improves its hardness and mechanical strength while increasing its work - hardening capacity, making it an ideal material for applications that demand high impact resistance and increased durability [8 - 14]. Specifically, the work - hardening property of manganese steel allows it to become harder under repetitive impacts, enhancing its resistance to deformation and wear over time. However, despite its high hardness which ensures good wear resistance this characteristic also tends to make the material more brittle, necessitating specific heat treatments to optimize its balance between hardness and toughness [15 - 18].

Heat treatments allow for modifications to the microstructure of 12 % Mn steel, resulting in a homogeneous austenitic matrix with optimal carbide precipitation and dispersion, thereby enhancing performance in applications that demand tensile and fatigue resistance [19 - 21]. Beyond improving mechanical properties, these treatments can also mitigate undesirable surface effects, such as corrosion, wear, and fatigue, thus extending the steel's longevity [22].

Many studies have focused on optimizing heat treatments for Hadfield steels, highlighting their impact on microstructural and mechanical properties. For instance, Ashok Kumar et al. showed that following austenitization heat treatment at 1100°C, carbon and manganese depletion renders the matrix unstable, leading to the decomposition of the austenitic matrix into ferrite and $(Fe, Mn)_3C$ carbides [23]. R. Harzallah et al. observed that water quenching following solution treatment can stabilize the austenitic structure [24]. However, although the austenitic phase in Hadfield steel confers high impact resistance, it is not well - suited to frictional applications due to its relatively low wear resistance. In certain conditions, though, the austenite can undergo rapid work - hardening when subjected to an appropriate heat treatment, thus giving Hadfield steel excellent wear resistance after a period of use [25, 26].

Additionally, Sabzi et al. demonstrated that manganese acts as an austenite stabilizer in Hadfield steels, delaying the degradation of austenite at 700°C and forming Mn_3C and $(Fe, Mn)_3C$ - type carbides. Increasing the carbon content from 1 % to 1.4 % by weight raises the hardness and yield strength of these steels but significantly reduces their toughness and ductility. Adding chromium in amounts between 1 % and 2.5 % promotes the formation of complex $(Fe, Mn, Cr)_{23}C_6$ carbides within the grains, which greatly decreases the toughness of the steel. This element is often added to improve the wear resistance of austenitic manganese steels [27].

In a similar context, Mousavi Anijdan et al. studied the effect of cooling rate after heat treatment on the mechanical properties, fatigue resistance, precipitation, and fracture mode of Hadfield austenitic steel. Their results indicate that samples quenched in a salt bath exhibit Mn_3C precipitates and display lower hardness, yield strength, and tensile strength. However, this condition favours a more ductile fracture mode and enhances formability [28]. Finally, R. Zellagui et al. demonstrated that high - temperature quenching in an agitated salt bath (950 - 1150°C) can reduce or eliminate carbides in austenitic steels, thus increasing their hardness and wear resistance [29].

The objective of this work is to evaluate the mechanical properties of highly alloyed manganese steel used in the fabrication of hammers and crusher jaws. To achieve this, a series of heat treatments, including quenching in water and ice water at different austenitization temperatures (1025°C, 1050°C, 1075°C, and 1100°C), was applied to purpose - manufactured samples. Microstructural analysis and phase identification of these samples were conducted using scanning electron microscopy coupled with energy - dispersive spectroscopy (SEM - EDS) and X - ray diffraction (XRD). Vickers microhardness measurements, with a load of 200 g, were performed on the core and polished surfaces of the samples. Impact resistance of these specimens, derived from high - manganese steel hammers, was determined through resilience testing. Additionally, tribological behavior under loads of 15 N, 20 N, 30 N, and 40 N was assessed by measuring the wear rate using a circular motion tribometer.

This expanded version provides further background on the industrial context, highlights the specific properties of Hadfield steel, discusses the roles of alloying elements and heat treatments, and outlines the study's specific objectives and methods.

EXPERIMENTAL

The materials used

The material used is steel provided by the Algerian foundry Tiaret (ALFET) / Algeria in its as - cast state for the production of samples. The table below (Table 1) shows the chemical composition results using a Metavision 1008i metal power spectrometer.

A 12 % manganese steel, in the form of a small ingot, was initially forged and then air - cooled. The forged steel was subsequently cut into square shapes with dimensions of (55×10×10) mm³. These squares underwent heat treatments, beginning with a treatment at 930°C for 30 min. The objective of this initial treatment was to achieve complete austenitization of the steel, allowing for a homogeneous microstructure by promoting the uniform diffusion of manganese and carbon within the matrix. This step is crucial for optimizing the subsequent austenitization process, ensuring the formation of high - quality martensite after quenching. The practical aspect of maintaining this temperature for 30 min provides sufficient time for the material to stabilize, ensuring that the benefits of austenitization are fully realized while minimizing energy consumption compared to higher temperatures. Subsequently, the steel was subjected to austenitization temperatures of 1025°C, 1050°C, 1075°C, and 1100°C, each with a holding time of 15 min, followed by quenching in two cooling mediums: water and ice water. The heat treatments were conducted in a chamber furnace.

Fig. 1 illustrates the schematic of the heat treatment program for the 12 % Mn steel in relation to the temperatures and durations of the heat treatment.

These selected heat treatment cycles for the 12 % Mn steel are aimed at obtaining the optimal microstructure to enhance ductility as well as toughness and wear resistance.

Experimental characterization techniques

X - ray diffraction

The diffraction patterns were recorded using a PANalytical X'PERT PRO MRD diffractometer equipped with a copper anode X - ray tube. A recording time of 45 sec per standardized angular step of approximately 0.04 in 2 θ was used over the range extending from 30° to 120° (2 θ). The identification of the crystalline phases present was done by comparing the observed peaks with those in the PDF2 database using the X'Pert HighScore Plus software. The crystal parameters and mass percentages of the relevant phases were deduced from structural refinements using the Rietveld method with Rietica software.

Scanning electron microscope (SEM) with EDS micro-analysis

Microstructural observations of the 12 % Mn steel were carried out using a Philips - type SEM (FEI Quanta 200). Our samples were cut to appropriate dimensions. Energy - dispersive X - ray spectroscopy

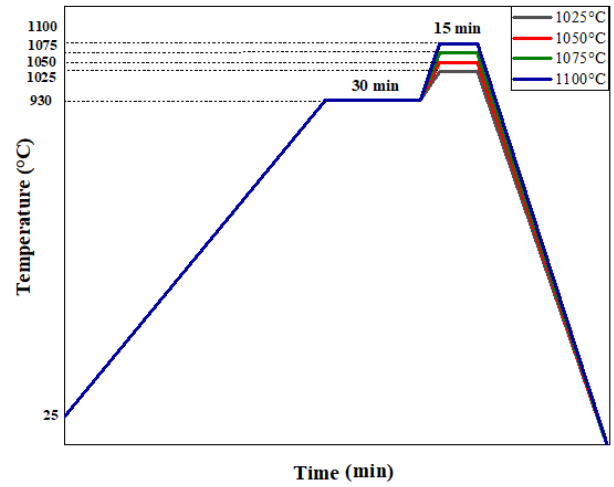

Fig. 1. Heat treatment cycles applied.

Table 1. Chemical Composition of 12 % Mn Steel, %.

%	C	Si	Mn	Cr	Fe	Mo	Ni	Cu
Acier 12 % Mn	1.19	0.3	12	2.36	85.79	0.163	0.239	0.124

(EDS) microanalysis was also performed on all samples to determine the chemical compositions of the various phases constituting the 12 % Mn steel.

Microhardness tests

Microhardness tests were conducted using a ZWICK HV microhardness tester equipped with a CCD camera enabling localized measurements with an approximate footprint size of 100 μm^2. Measurements were performed on polished surfaces using a Vickers indenter under a load of 200 g.

Resilience tests

The resilience test is intended to measure the energy required to fracture a notched specimen in a single stroke. The apparatus used is a pendulum impact tester (ZwickRoell) equipped with clamping and centering devices for the specimens, as well as a dial where the energy in joules is recorded after fracture of the specimen. The specimens used have dimensions of 10 x 10 x 55 mm^3 with a V - notch at 45°. The energy absorbed by the specimen is calculated using the Eq. (1):

$$W = P\,(h_0 - h_1) \quad (1)$$

where: P: is the weight of the pendulum; h_0: is the initial height at which the pendulum is positioned; h_1: is the height to which the pendulum rises after fracture of the specimen.

Resilience (expressed in J cm^{-2}) is calculated as the ratio of the absorbed energy W to the cross, sectional area of the specimen at the point of fracture.

Tribological testing

Tribological tests were conducted on the samples using a “pin - on - disc” type device. Its principle involves applying a load on the stationary pin in the horizontal plane in contact with the surface of a rotating disc along the vertical axis (Fig. 2). The disc, made of 100 Cr6 steel with a hardness of 62 HRC, has a rubbing surface diameter of 3 mm. It rotates at a constant speed. A static normal load N is applied to it. As a result of this load on the pin and the sliding speed of the latter, a friction force F_t appears at the point of contact between the pin and the disc. The wear of the pins is evaluated using the weighing method (precision balance of 10^{-5} g)

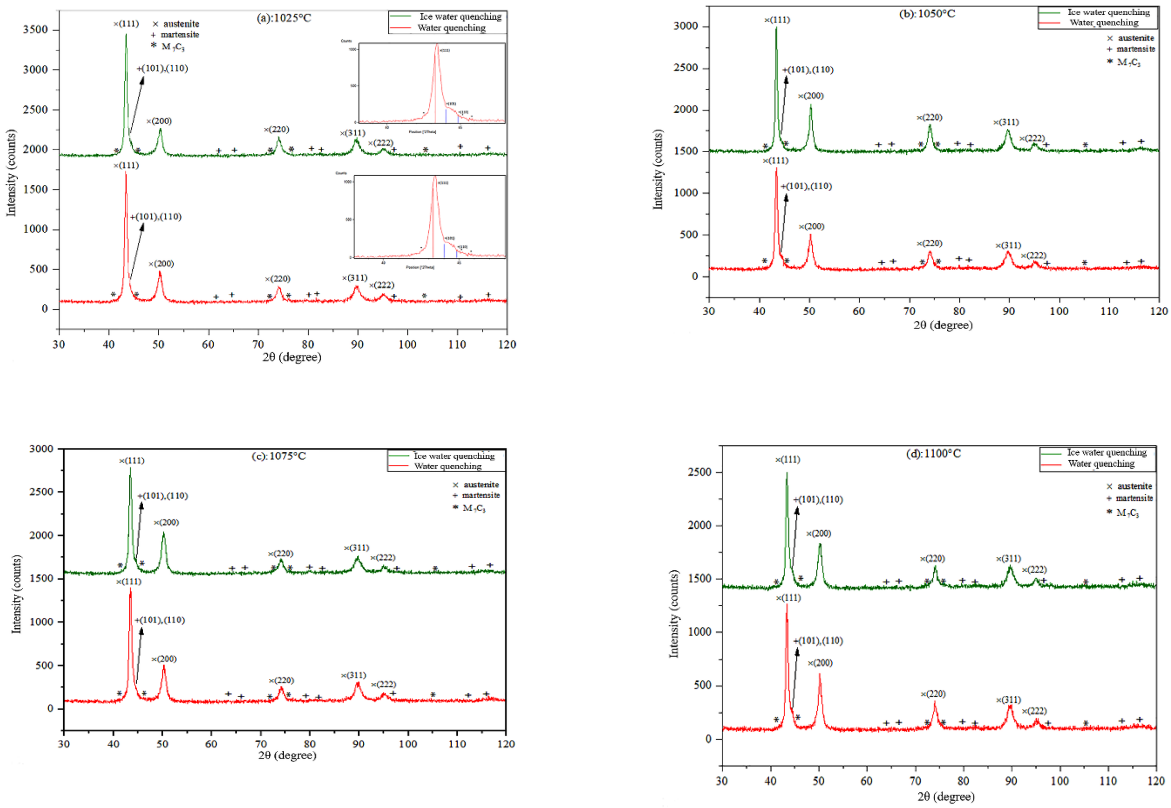

Fig. 2. Diffractograms of 12 % Mn steel: (a) - treated at 1025°C; (b) - 1050°C; (c) - 1075°C; (d) - 1100°C.

before and after each test.

The rate of wear and tear is calculated according to Eq. (2):

$$K_v = \Delta m \; N_c^{-1} \quad (2)$$

where: K_v: Wear rate; Δm: Relative mass loss; N_c: Number of cycles performed during the test, measured using an integrated sensor that automatically detects each complete cycle.

The test conditions are as follows:

Relatively dry ambient environment (20°C to 23°C); Normal loads of 15 N, 20 N, 30 N, and 40 N; Sliding speeds: 0.5 m s^{-1} and 1 m s^{-1}; Sliding distance: 900 m and 1800 m; Test duration: 30 min.

RESULTS AND DISCUSSION

X - ray diffraction structural analysis of 12 % Mn steel

Fig. 2 shows the diffractograms of different heat - treated 12 % Mn steel samples quenched with water and ice water: a) 1025°C; b) 1050°C; c) 1075°C and 1100°C.

One notices the presence of three common phases in all samples. The main phase identified is the solid solution of austenite type with a face - centered cubic structure ((JCPDS nº. 052 - 0512); refining its crystalline parameter yields a value of a = 3.6225 (6) Å, with very low fluctuations from one sample to another related to the distribution of elements in the different phases. The second phase is martensite of tetragonal symmetry (JCPDS nº. 044 - 1292); it is notable that its main peaks, specifically (101) and (110), partially overlap at the base of the (111) peak of the austenite phase. Refinement of its crystalline parameters gives a = 2.885 (3) Å and c = 2.987 (4) Å. The third very minor phase is carbide of formula M_7C_3 (e.g., JCPDS nº. 075 - 1499) with M representing the metallic elements in the composition, particularly Fe, Mn, and Cr, and the Carbon site potentially allowing partial substitution with the element Si. The presence of this carbide is linked to the partial transformation of austenite into martensite. The high number of its peaks in relation to the size of the crystal lattice precludes the depiction of diffraction orders on the diagrams; instead, their approximate positions are indicated by *. The low intensities of its peaks did not allow for the refinement of the crystalline parameters of this orthorhombic symmetry structure; however, they are expected to be slightly larger than those of the Fe_7C_3 phase (a = 4.5370 Å, b = 6.8920 Å, and c = 11.9130 Å) due to the slightly larger sizes of Mn and Cr atoms compared to Fe. This is the same reason behind the slight increase in the crystalline parameters of the austenite and martensite phases in our samples compared to the usual Fe - based phases. This indicates that the different metallic elements of the composition are more or less distributed among the three present phases: austenite, martensite, and M_7C_3 carbide.

Fundamentally, the scale constants of the phases deduced from structure refinement by the Rietveld method allow for quantitative phase analysis with very high precision, even in the presence of specific complications such as preferred orientation. Due to the very low intensities of the M_7C_3 phase, its inclusion in such refinements would lack precision, and the obtained values would be meaningless. Therefore, the qualitative analysis of phases in our samples concerns only the austenite and martensite phases, and the deduced percentages (Fig. 3) are comparative between these two phases, yet still representative overall given the very low content of M_7C_3 - type carbides.

The phase quantification of the heat - treated samples, quenched in water and ice water, primarily consists of a main austenitic phase, which is a face - centered cubic (FCC) solid solution. For the samples quenched in water at austenitization temperatures of 1025°C, 1050°C, 1075°C, and 1100°C, their martensite content is respectively 7.5 %, 7.9 %, 11.5 %, and 15.9 %. Conversely, for the samples treated at 1025°C, 1050°C, 1075°C, and 1100°C and then quenched in ice water, the proportions of present martensite are 7.3 %, 8.2 %, 11.9 %, and 16.6 %, respectively. However, the austenite fraction in the samples quenched in ice water has been reduced compared to those quenched in water. This is due to the ice water quenching, which has further favored martensite formation.

SEM characterization of 12 % manganese steel

The microstructures of the samples treated at (1025°C, 1050°C, 1075°C, 1100°C) and quenched in water and ice water are obtained by scanning electron microscopy (SEM) coupled with EDS microanalysis to detect and identify the chemical composition of the structural components of the 12 % Mn steel, as shown in Figs. 4 - 7.

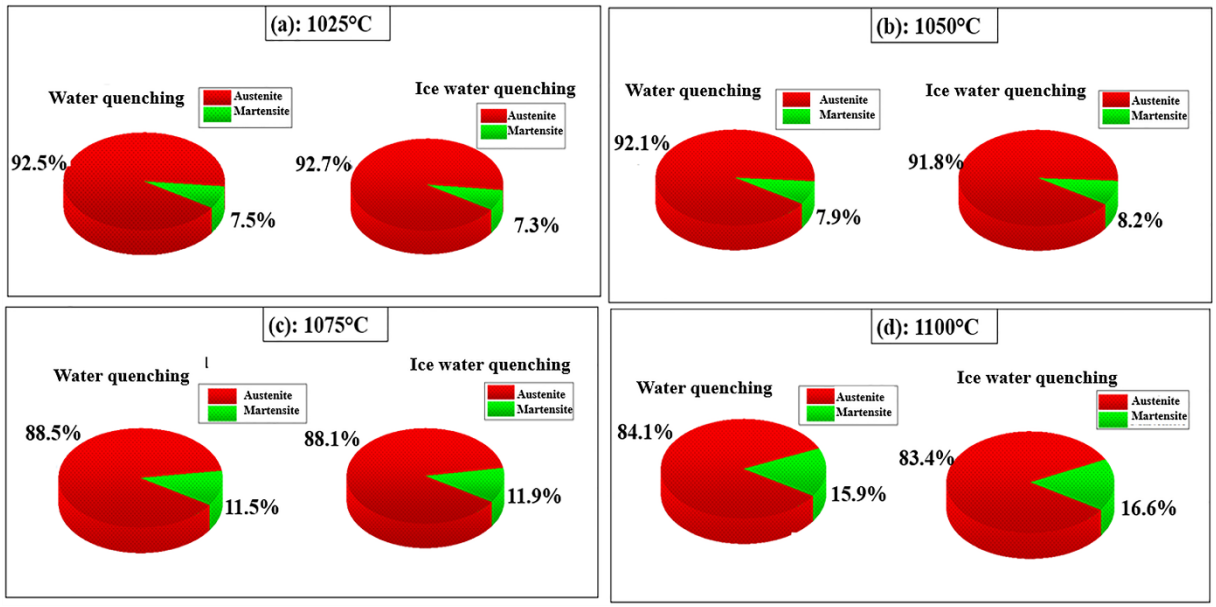

Fig. 3. Quantification of the phases of 12 % Mn steel: (a) - treated at 1025°C; (b) - 1050°C; (c) - 1075°C; (d) - 1100°C.

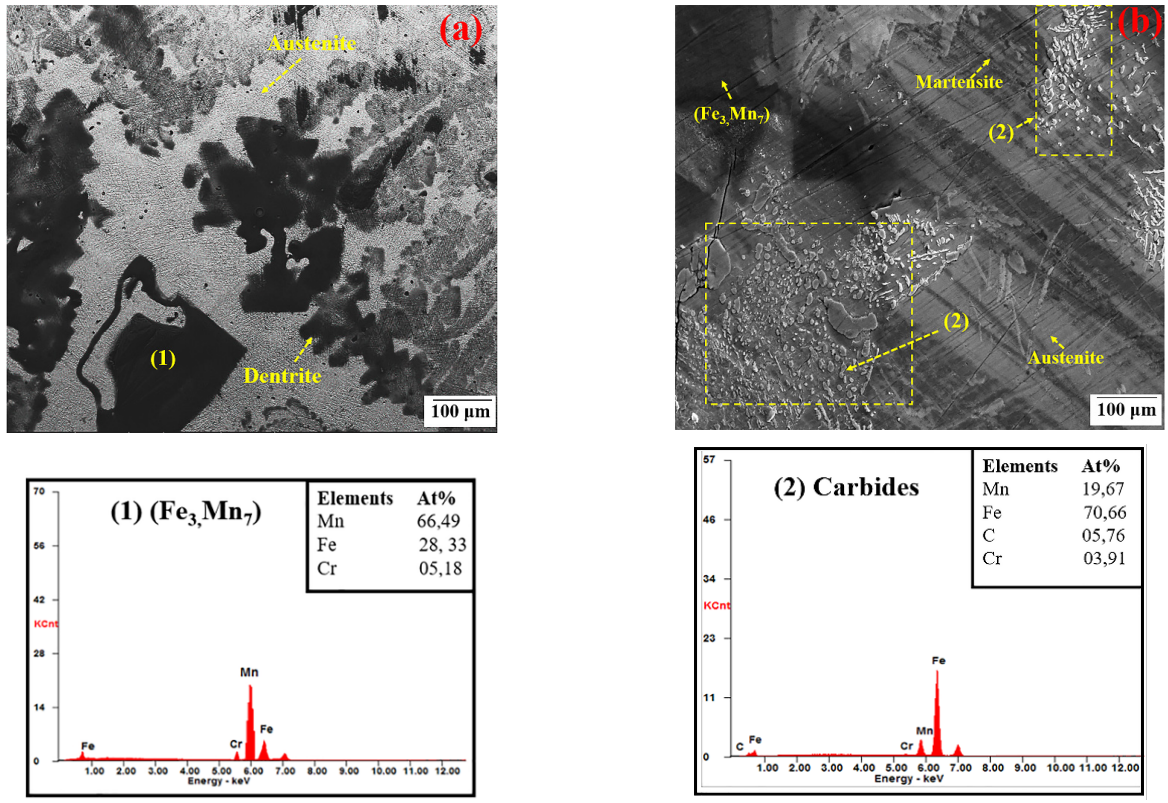

Fig. 4. SEM micrograph coupled with EDS microanalysis of 12 % Mn steel treated at 1025°C; (a) water-quenched; (b) ice-cold water-quenched.

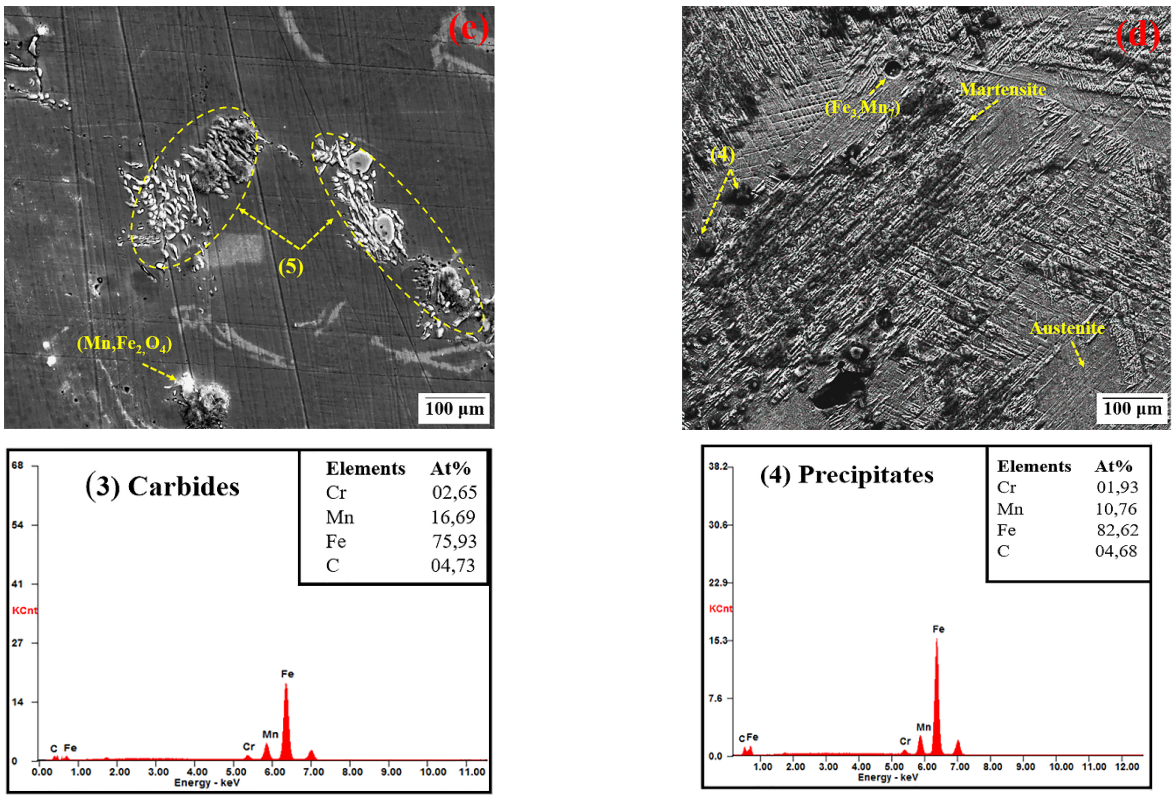

Fig. 5. SEM micrograph coupled with EDS microanalysis of 12 % Mn steel treated at 1050°C; (c) water-quenched; (d) ice-cold water-quenched.

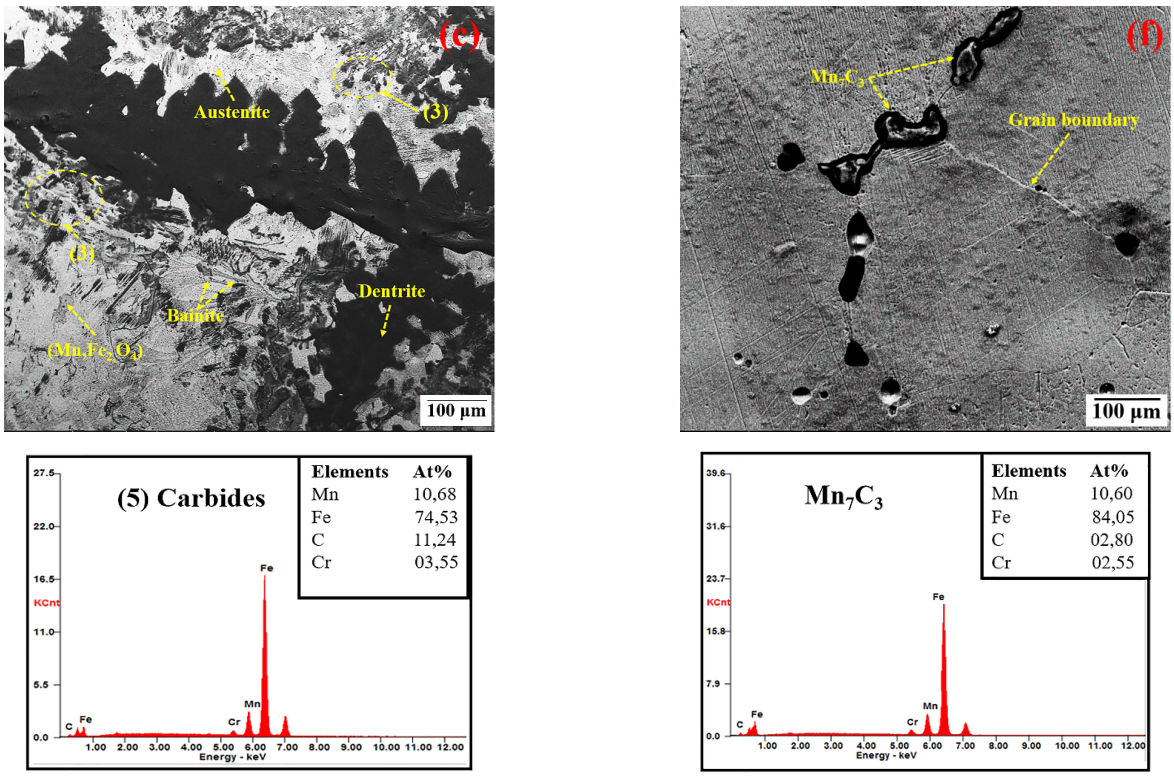

Fig. 6. SEM micrograph coupled with EDS microanalysis of 12 % Mn steel treated at 1075°C; (e) water-quenched; (f) ice-cold water-quenched.

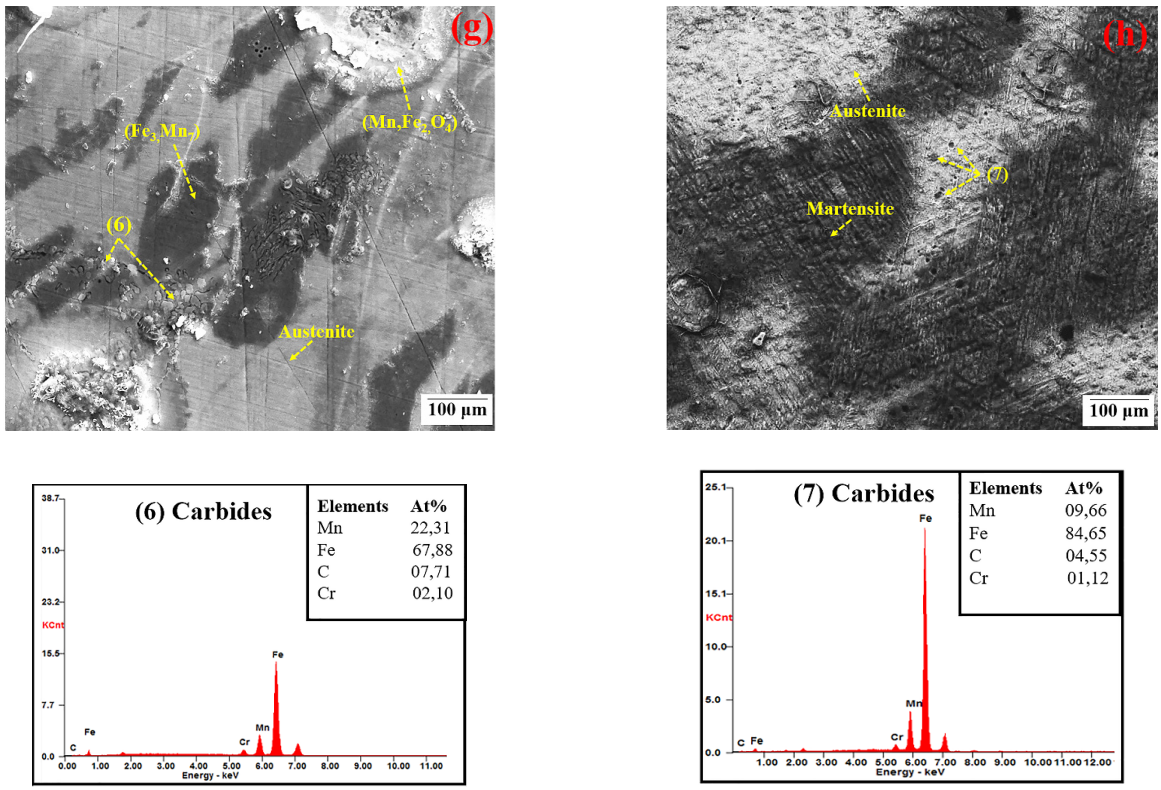

Fig. 7. SEM micrograph coupled with EDS microanalysis of 12 % Mn steel treated at 1100°C; (g) water-quenched; (h) ice-cold water-quenched.

The microstructural analysis reveals differences in the phases present in manganese steel, depending on the heat treatment temperature and the cooling medium used. In Fig. 4a, the steel treated at 1025°C and quenched in water predominantly exhibits an austenitic matrix, characterized by its excellent ductility and toughness. However, the presence of the intermetallic compound Fe_3Mn_7, along with a small amount of (Fe, Mn) C - type carbides, indicates a complex interplay among the elements during cooling. This intermetallic compound can enhance certain mechanical properties, such as strength, but may also contribute to brittleness if present in excess.

On the other hand, the microstructure illustrated in Fig. 4b, resulting from quenching in ice water, displays the formation of M_7C_3 - type carbide precipitates. The precipitation of M_7C_3 is noteworthy as it not only contributes to the overall hardness of the material but also indicates a depletion of carbon and manganese in the austenitic matrix. The depletion of manganese, a stabilizing element for the austenitic phase, introduces instability, potentially leading to the decomposition of austenite into ferrite and M_7C_3 carbides. This transformation can adversely affect the toughness of the material if the decomposition is significant.

Additional insights can be derived from the heat treatment at 1050°C, as shown in Fig. 5c. The presence of a predominant austenitic phase alongside a bainitic microstructure suggests that the transformation of austenite into martensite was not fully complete. The bainitic structure is characterized by a fine microstructure that can enhance toughness compared to coarser microstructures. However, the incomplete transformation also implies that the steel may not reach its maximum hardness potential, which is a critical consideration for applications requiring high wear resistance.

In contrast, Fig. 5d illustrates the microstructure of the steel quenched in ice water after the same heat treatment. Here, the presence of martensite, along with precipitates attributed to the continuous formation of M_7C_3 carbides along the grain boundaries, indicates a more favourable scenario for achieving increased hardness and wear resistance. The martensitic phase

contributes to the overall hardness of the steel, while the precipitation of M_7C_3 carbides along the grain boundaries can impede dislocation movement, thereby improving wear resistance. These grain boundaries constitute the most active zones for the growth of precipitates. Regarding the heat treatment undergone at 1075°C, the microstructure of the manganese steel quenched in water exhibits zones composed solely of carbide aggregates, as shown in Fig. 6e. In this context, degenerated pearlite can also be observed, indicating incomplete transformation and affecting the overall mechanical properties of the steel. Meanwhile, the sample quenched in ice water displays a microstructure formed of M_7C_3 - type carbides that are dispersed along grain boundaries with a homogeneous distribution. This homogeneity results from the decomposition of larger carbides into M_7C_3 carbides, as seen in Fig. 6f. The presence of degenerated pearlite alongside these carbide structures highlights the complex interplay of phases that can influence the performance characteristics of the steel, particularly in terms of its hardness and wear resistance.

Fig. 7g displays a structure similar to that of the samples subjected to heat treatment at 1025°C, 1050°C, and 1075°C, and quenched in water, with a higher proportion of the intermetallic compound (Fe_3, Mn_7) and complex oxide type (Mn, Fe_2, O_4). Conversely, the sample subjected to heat treatment at 1100°C followed by quenching in ice water exhibits a compact microstructure with the formation of martensite and small carbides uniformly distributed in the austenitic matrix as indicated in Fig. 7h [32].

Microhardness measurements

The microhardness at the core and surface of the various heat - treated samples at different austenitization temperatures (1025°C, 1050°C, 1075°C, and 1100°C) followed by quenching in water and ice water was measured using Vickers indentation with a 200 g load for 10 s.

Fig. 8 depicts the evolution of Vickers microhardness at the core and surface of the different heat - treated samples quenched in water and ice water for 12 % Mn steel.

The microhardness values measured at the core of the 12 % Mn samples (Fig. 8a) show fluctuations depending on the quenching method. For samples quenched in water without tempering, the values range from 341 $HV_{0.2}$ to 405 $HV_{0.2}$, while those quenched in ice water range from 312 $HV_{0.2}$ to 322 $HV_{0.2}$. In comparison, the microhardness values on the surface of the 12 % Mn samples (Fig. 8b) are approximately 410 $HV_{0.2}$ to 515 $HV_{0.2}$ for samples quenched in water and 436 $HV_{0.2}$ to 680 $HV_{0.2}$ for those quenched in ice water.

Based on the results obtained, it is observed that the microhardness values at the surface of the 12 %

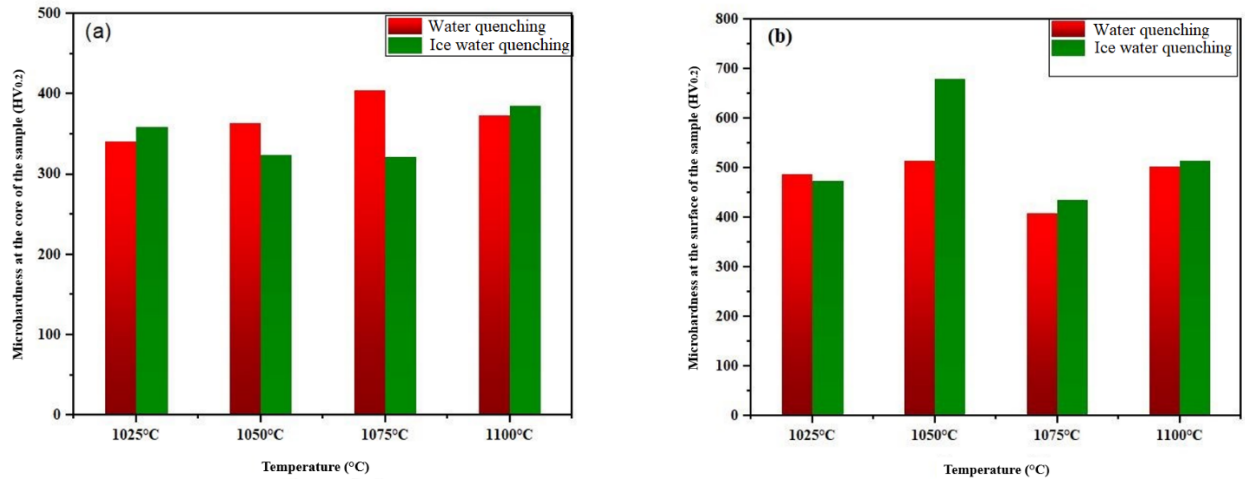

Fig. 8. Influence of austenitization temperature and cooling medium on the hardness of 12 % Mn steel: (a) core of 12 % Mn sample, (b) surface of 12 % Mn sample.

Mn sample are higher than those at its core. For samples quenched in water, the values are 341 $HV_{0.2}$ and 515 $HV_{0.2}$, respectively, while for those quenched in ice water, the values are 312 $HV_{0.2}$ and 680 $HV_{0.2}$, respectively. The improvement in the hardness of the 12 % Mn steel for samples subjected to quenching in ice water is attributed to the impact of the heat treatment. Indeed, this treatment promotes the formation of fine - grained M_7C_3 carbides as well as martensite. These carbides are uniformly distributed across the entire sample surface. In contrast, the carbides detected in samples quenched in water are larger - grained and distributed indiscriminately within the austenitic matrix.

The microhardness at the core of the sample ranges from 312 to 405 $HV_{0.2}$. The sample treated at 1050°C and quenched in ice water displayed the lowest microhardness value of 312 $HV_{0.2}$. In contrast, the sample treated at 1075°C and quenched in water exhibited the highest value, which is 405 $HV_{0.2}$. However, the microhardness of the sample surfaces ranged from 410 to 680 $HV_{0.2}$. The sample treated at 1075°C and quenched in water showed the minimum microhardness value of 410 $HV_{0.2}$. Conversely, the highest value of 680 $HV_{0.2}$ was obtained for the sample treated at 1050°C and quenched in ice water. The microhardness values at the core are lower than those at the surface of the 12 % Mn steel. This is because the toughness of the carbide formed on the sample surface is higher than that of the austenitic phase at the core of the sample, as carbides are hard particles that improve hardness and wear resistance [27]. This finding is supported by the study of Rodrigo Lencina et al. who investigated the influence of manganese in steels containing 12 % Mn and 16 % Mn on a macro scale of a real component, as well as on the metallographic structure and microhardness of the quenched portion of a manganese austenitic steel. Their study, based on microhardness profiles for two compositions studied, showed a clear difference between the microhardness values measured at the surface and at the core of the analysed samples. At the surface, microhardness varies between 600 - 700 $HV_{0.2}$, whereas at the core it is equal to 300 $HV_{0.2}$ [33].

Impact resistance test

Fig. 9 presents the impact tests conducted on samples treated at austenitizing temperatures of 1025°C, 1050°C, 1075°C, and 1100°C, using two different cooling media (water and ice water).

The results obtained (Fig. 9) show that the sample treated at 1050°C and quenched in ice water exhibits excellent impact resistance, with the highest resilience value of approximately 161.27 J cm^{-2}. In contrast,

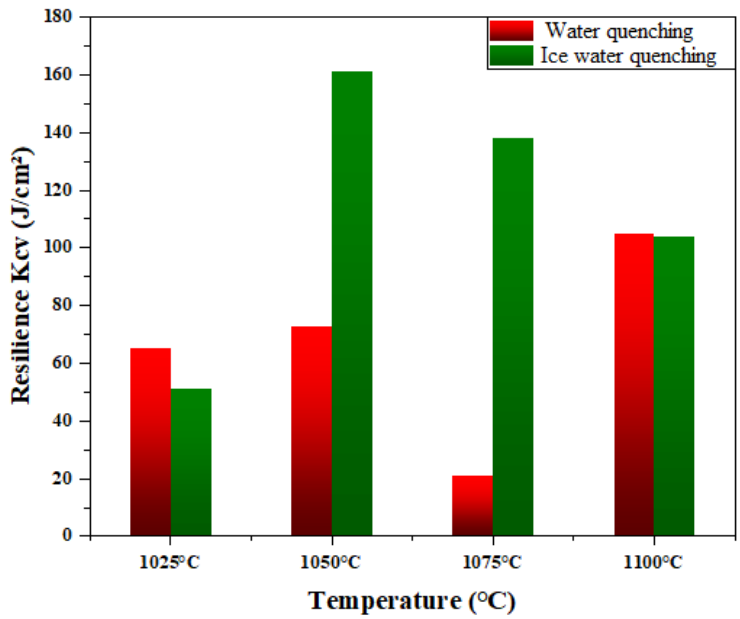

Fig. 9. Effect of heat treatment on impact resistance.

for the samples quenched in water, the maximum resilience value is observed for the heat treatment at 1100°C, reaching around 105 J cm^{-2}. This difference can be explained by the grain size of the carbides and their distribution on the material's surface. Indeed, the Mn_7C_3 carbides present in the samples quenched in ice water are fine - grained and uniformly distributed at the joints of the austenitic matrix, thereby enhancing impact resistance. Conversely, in the samples quenched in water, the large - grained carbides formed are randomly distributed within the austenitic matrix, thus deteriorating the mechanical properties of the material, particularly resilience. This observation is consistent with the results obtained from X - ray diffraction (XRD) and scanning electron microscopy (SEM).

Tribological test results

Wear tests were conducted under dry conditions with different loads (15 N, 20 N, 30 N, and 40 N) and two sliding speeds (0.5 m s^{-1} and 1 m s^{-1}) for a duration of 30 min.

Fig. 10 illustrates the results obtained from wear tests performed on samples treated at temperatures of 1025°C, 1050°C, 1075°C, and 1100°C, followed by quenching in water and ice water.

The sample treated at 1050°C and quenched in ice water, under a sliding speed of 1 m s^{-1}, exhibits a low wear rate of approximately (0.23 × 10^{-4} mg m^{-1}). This is attributed to the uniform dispersion of M_7C_3

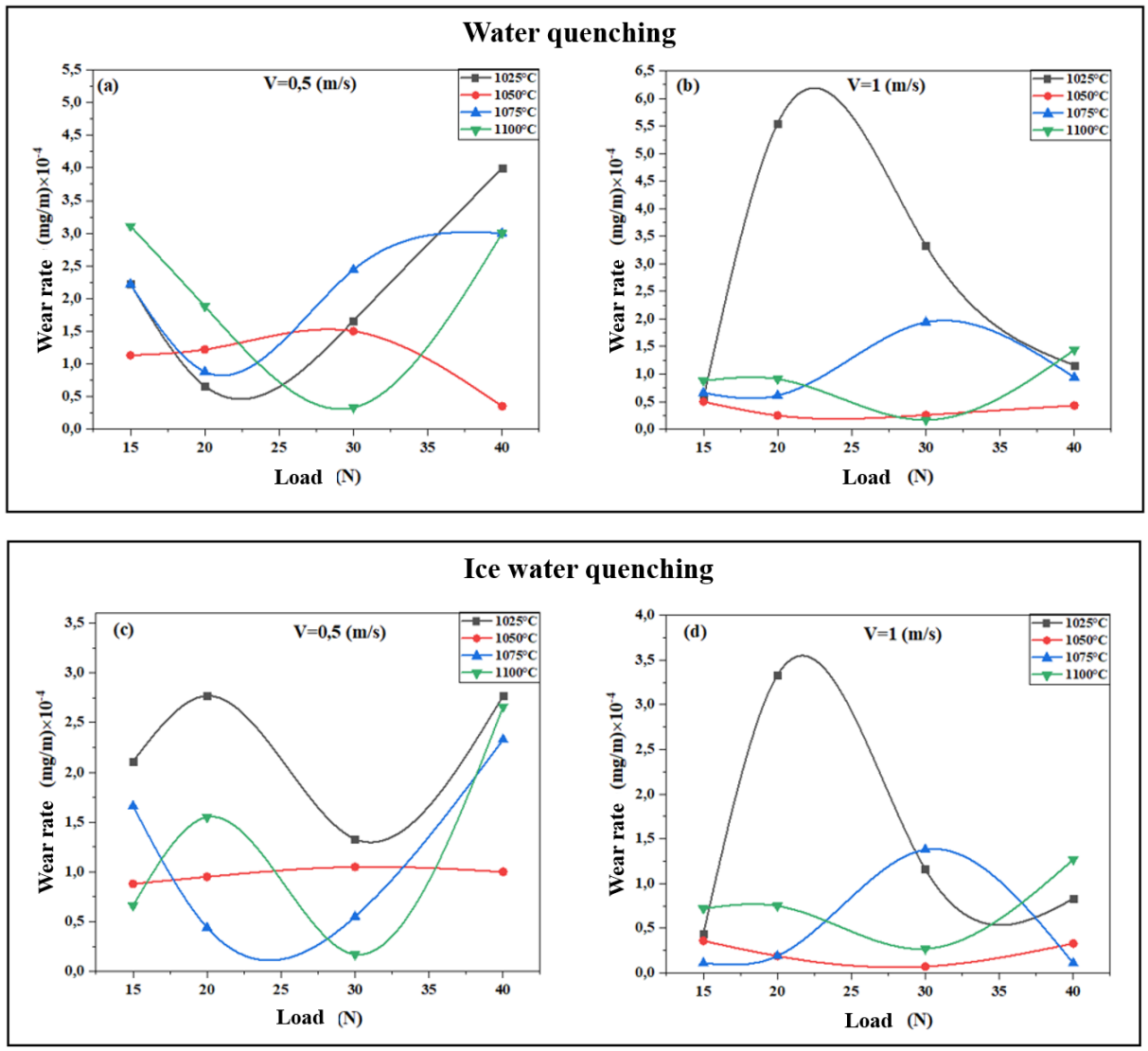

Fig. 10. Wear rate of samples at different austenitization temperatures as a function of sliding speed, (a) 0.5 m s^{-1}; (b) 1 m s^{-1} water quenched; (c) 0.5 m s^{-1}; (d) 1 m s^{-1}. quenched in ice-cold water.

carbides, which enhances the hardening of the steel, thereby improving its wear resistance. Furthermore, this hardening after heat treatment is also due to the formation of martensite resulting from microstructural changes associated with the transformation of austenite into martensite, thus enhancing the wear behavior of the studied manganese steel.

Mehdi Mazar Atabaki et al. compared the wear behaviour of manganese austenitic steel to that of high - chromium cast iron. It was deduced from this study that manganese austenitic steel consistently exhibits the best wear results across different loads [34]. The same observation applies to the sample austenitized at 1050°C and quenched in both water and ice water, under sliding speeds of 0.5 m s^{-1} and 1 m s^{-1}, showing a stabilization of the wear rate for all applied loads (15 N, 20 N, 30 N, and 40 N) (Fig. 10). However, the sample treated at 1050°C and quenched in water, under a sliding speed of 1 m s^{-1}, exhibits a wear rate of approximately (0.36×10^{-4} mg m^{-1}), which is slightly higher than that of the sample treated at 1050°C and quenched in ice water. This can be explained by a sliding mechanism that leads to the rupture of asperities due to the presence of larger carbides.

The wear rate for the heat treatment at 1025°C followed by water quenching increases during the test for both sliding speeds. This is attributed to the material removal phenomenon observed throughout the tribological test, which contributed to degrading the surface properties of the samples and, consequently, their tribological performance.

CONCLUSIONS

This study focuses on the microstructural, structural, and mechanical characterization of 12 % manganese steel intended for the manufacturing of hammers and crushing jaws in the mining industry. The key findings can be summarized as follows:

- X - ray Diffraction analysis: All samples exhibited a solid solution of austenite. The presence of martensite and M_7C_3 - type carbides was confirmed in samples quenched in water and ice water.
- SEM Microstructural analysis: Water - quenched manganese steel displayed large carbide aggregates within an austenitic matrix, while ice water - quenched steel showed a compact microstructure with martensite and finely dispersed Mn_7C_3 carbides.
- Microhardness measurements: The lowest microhardness value of 312 $HV_{0.2}$ was recorded for the sample treated at 1050°C and quenched in ice water.
- Resilience tests: The sample treated at 1050°C and quenched in ice water achieved an impact resistance of approximately 161.27 J cm^{-2}, attributed to the fine - grained Mn_7C_3 carbides at the austenitic matrix boundaries.
- Wear resistance: The same sample, under a sliding speed of 1 m s^{-1}, demonstrated improved wear resistance with a wear rate of approximately $0.3.10^{-4}$ mg m^{-1}.
- Tribological behavior: The sliding speed and contact pressure have influenced wear rates; the treatment at 1050°C followed by quenching in ice water yielded the optimal microstructure for tribological performance.

These results highlight the significance of the selected austenitization temperature, particularly the 1050°C treatment, which enhanced mechanical properties. The recommendations derived from this study will be valuable for foundries producing this material, thereby meeting the industry's expectations.

Acknowledgements

The work described in this article was conducted as part of a project within our laboratory team. We would like to express our deep gratitude to the Algerian foundry Tiaret (ALFET) Algeria, which provided assistance in delivering the steel for investigation.

Authors' contributions

S.K.: Carried out the heat treatments, mechanical tests, and tribological analyses, while also contributing to the manuscript writing. R.Y.: Supervised the experimental tests. T.J.: Analysed the results and assessed the wear resistance. A.S.: Designed the study, coordinated the project, validated the analyses, and critically reviewed the manuscript. M.A.B.: Participated in the writing and revision of the manuscript. A.B.: Performed the microstructural characterization using SEM/EDS and XRD, as well as the interpretation of the X - ray diffraction results.

REFERENCES

1. M.K. Pham, D.N. Nguyen, A.T. Hoang, Influence of vanadium content on the microstructure and mechanical properties of high-manganese steel, Int. J. Mech. Mechatronics Eng., 18, 2, 2018, 141-147. https://doi.org/10.1007/s41230-021-1002-1
2. R. Dalai, S. Das, K. Das, Relationship between the microstructure and properties of thermomechanically processed Fe-17Mn and Fe-17Mn-3Al steels, Int. J. Miner. Metall. Mater., 26, 2019, 64-75. https://doi.org/10.1007/s12613-019-1710-3
3. S. Mohapatra, G. Poojari, S. Das, K. Das, Insights into the dynamic impact behavior of intercritically annealed automotive-grade Fe-7Mn-4Al-0.18C steel, Mater. Sci. Eng. A, 887, 2023, 145769. https://doi.org/10.1016/j.msea.2023.145769
4. R. Dalai, S. Mohapatra, S. Das, K. Das, Effect of thermo-processing on the microstructure, impact abrasion wear, and corrosion resistance properties of TiC reinforced Al-added high-Mn steel matrix composite, JOM, 75, 12, 2023, 5281-5289. https://doi.org/10.1007/s11837-023-05974-5
5. J. Kowalsk, J. Ryś, A. Radziszewska, Favourable conditions for strain induced transformations in unstable high-manganese steel, Mater. Charact., 2024, 113884. https://doi.org/10.1016/j.matchar.2024.113884
6. C. Chen, B. Lv, H. Ma, D. Sun, F. Zhang, Wear behavior and the corresponding work hardening characteristics of Hadfield steel, Tribol. Int., 121, 2018, 389-399. https://doi.org/10.1016/j.triboint.2018.01.044
7. M.K. ElFawkhry, Thermoplastic deformation of ladle-treated Hadfield steel with free crack susceptibility, Int. J. Met., 15, 2021, 1348-1361. https://doi.org/10.1007/s40962-020-00567-3
8. M. Sabzi, F. Mansour, Hadfield manganese austenitic steel: a review of manufacturing processes and properties, Mater. Res. Express, 6, 10, 2019, 1065c2. https://doi.org/10.1088/2053-1591/ab3ee3
9. X. Jincheng, Ecodesign for wear resistant ductile cast iron with medium manganese content, Mater. Des., 24, 1, 2003, 63-68. https://doi.org/10.1016/S0261-3069(02)00076-6
10. N.H. Hai, N.D. Trung, P.M. Khanh, N.H. Dung, B.D. Long, Strain hardening of Hadfield high manganese steels, Mater. Today Proc., 2022, 2933-2937. https://doi.org/10.1016/j.matpr.2022.06.561
11. S. Wen, Y. Xie, H. Zhang, G. Wang, Z. Li, Strain hardening behavior and mechanical properties of Hadfield steel subjected to severe plastic deformation, Mater. Sci. Eng. A, 789, 2020, 139554. https://doi.org/10.1016/j.msea.2020.139554
12. L. Zhang, X. Lei, Y. Su, L. Yu, R. Liu, J. Lu, Enhancing the impact toughness of Hadfield steel by grain refinement and dynamic recrystallization, Mater. Sci. Eng. A, 812, 2021, 141136. https://doi.org/10.1016/j.msea.2021.141136
13. M.C. Somani, L.P. Karjalainen, J. Honkanen, H. Hänninen, High-strain-rate deformation behavior of Hadfield steel at elevated temperatures, J. Mater. Process. Technol., 214, 2014, 2288-2295. https://doi.org/10.1016/j.jmatprotec.2014.04.015
14. T.S. Dhandapani, K. Ravi, V.S. Rao, K.S. Prasad, B.S. Murty, Influence of grain size on the wear behavior of Hadfield manganese steel, Wear, 428-429, 2019, 366-375. https://doi.org/10.1016/j.wear.2019.03.002
15. Y. Zhang, B. Guo, J. Liu, Z. Sun, Effects of cryogenic treatment on the microstructure and properties of Hadfield steel, Mater. Sci. Eng. A, 823, 2021, 141766. https://doi.org/10.1016/j.msea.2021.141766
16. S.R. Patil, B.M. Mahato, S.N. Ojha, Effect of heat treatment on the mechanical properties of Hadfield steel, Mater. Today Proc., 26, 2020, 3370-3374. https://doi.org/10.1016/j.matpr.2020.02.695
17. A. Kumar, A.K. Bhagat, D.P. Mondal, K. Das, S. Das, Influence of carbide reinforcement on the wear resistance of high-manganese steel, J. Mater. Res. Technol., 9, 2020, 11604-11612. https://doi.org/10.1016/j.jmrt.2020.08.009
18. H. Liu, X. Li, J. Wu, M. Zhang, Effect of grain refinement on the impact toughness of Hadfield steel, Mater. Sci. Eng. A, 753, 2019, 216-223. https://doi.org/10.1016/j.msea.2019.03.113
19. Y. Zhang, H. Li, J. Wu, R. Liu, Effect of grain boundary engineering on the mechanical properties of Hadfield steel, Mater. Sci. Eng. A, 769, 2020, 138540. https://doi.org/10.1016/j.msea.2019.138540
20. B.L. Mordyuk, Y.V. Levchenko, M.A. Iefimov, V. I. Ivanov, Enhancement of Hadfield steel properties by ultrasonic impact treatment, Mater. Sci. Eng. A, 477, 1-2, 2008, 153-162. https://doi.org/10.1016/j.

msea.2007.05.048
21. K.H. Lo, C.H. Shek, J.K.L. Lai, Recent developments in stainless steels, Mater. Sci. Eng. R Rep., 65, 2009, 39-104. https://doi.org/10.1016/j.mser.2009.03.001
22. M.E. Kassner, M.T. Pérez-Prado, Fundamentals of creep in metals and alloys, Elsevier, 2004, 133-136. https://doi.org/10.1016/B978-0-08-044373-7.X5000-6
23. P.K. Samal, R.E. Schafrik, Powder metallurgy: fundamentals and case studies, Elsevier, 2014, 217-225. https://doi.org/10.1016/B978-0-12-401682-8.00009-4
24. T. Gladman, Precipitation hardening in metals, Mater. Sci. Technol., 15, 1999, 30-36. https://doi.org/10.1179/026708399773002782
25. G.B. Olson, M. Cohen, A mechanism for the strain-induced nucleation of martensitic transformations, J. Less Common Met., 28, 1972, 107-118. https://doi.org/10.1016/0022-5088(72)90089-1
26. F.G. Caballero, C.G. de Andres, F.G. Jimenez-Melero, J. Chao, M. Kuntz, C. Garcia-Mateo, New experimental evidence on strain-induced martensitic nucleation in austenitic steels, Acta Mater., 55, 2007, 381-390. https://doi.org/10.1016/j.actamat.2006.07.046
27. L. Remy, Temperature and strain rate dependence of work hardening and of flow stress of iron and steel, Mater. Sci. Eng., 28, 1977, 99-107. https://doi.org/10.1016/0025-5416(77)90166-3
28. H.K.D.H. Bhadeshia, Bainite in steels: theory and practice, CRC Press, 2001, 94-98. https://doi.org/10.1201/9781420030037
29. A.J. Clarke, S.V. Ushakov, J.T. Czajkowski, D.A. Hughes, High-temperature deformation behavior of transformation-induced plasticity steels, Metall. Mater. Trans. A, 35, 2004, 1613-1622. https://doi.org/10.1007/s11661-004-0222-9
30. D.K. Matlock, G. Krauss, Influence of composition and microstructure on the strength and toughness of transformation-induced plasticity steels, Metall. Mater. Trans. A, 13, 1982, 1365-1373. https://doi.org/10.1007/BF02642459
31. J.O. Nilsson, Super duplex stainless steels, Mater. Sci. Technol., 8, 1992, 685-700. https://doi.org/10.1179/mst.1992.8.8.685
32. H.W. Hayden, W.G. Moffatt, J. Wulff, The structure and properties of materials, Vol. III: Mechanical behavior, Wiley, 1965, 135-139. https://doi.org/10.1002/9780470248874
33. G. Thomas, R.F. Mehl, The nucleation and growth of deformation twins in metals: part I, Acta Metall., 1, 1953, 133-140. https://doi.org/10.1016/0001-6160(53)90034-6
34. P.L. Mangonon, G. Thomas, The martensite phases in 304 stainless steel, Metall. Trans., 1, 1970, 1577-1586. https://doi.org/10.1007/BF03037856